Multi-level assessment of the ASR damage including Vickers' hardness in concrete

Diego Jesus de Souza [(1)], Leandro F. M. Sanchez [(2)]

(1) University of Ottawa, Ottawa, Canada, dsouz025@uottawa.ca

(2) University of Ottawa, Ottawa, Canada, Leandro.Sanchez@uottawa.ca

Abstract

Alkali-Silica Reaction (ASR) is one of the most harmful distress mechanisms affecting the durability and serviceability of concrete infrastructure worldwide. Over the past decades, several engineers and researchers around the globe have tried to develop measures in the laboratory and in the field to assess the damage caused by ASR. Yet, very few researches have been conducted on the understanding of the elastic properties of ASR-gel and it is anticipated that its inner features such as mechanical properties might play an important role in induced damage of affected structural components presenting distinct exposure conditions and confinement effects. This research presents the results of a multi-level assessment of ASR-induced expansion and damage and focuses on the distress caused within distinct locations of affected concrete; i.e. aggregate particles, ITZ and cement paste. Moreover, an overall characterization of the mechanical properties of ASR-gel is performed through the use of the micro-indentation technique to better understand ASR-gel features at distinct zones and expansion levels. Such assessment allows the development of comprehensive and quantitative data enabling a better understanding of the material's deterioration as a function of ASR development.

Keywords*: alkali-silica reaction; the durability of concrete; micro-indentation; overall assessment of the damage*

1. INTRODUCTION

Alkali-Silica Reaction (ASR) is one of the most harmful distress mechanisms affecting the durability and serviceability of concrete infrastructure worldwide. ASR is conventionally defined as a chemical reaction between the alkali hydroxides (i.e. Na^+, K^+ and OH^-) dissolved in the concrete pore solution and some reactive mineral phases containing reactive silica forms present in the aggregates used in the mixture [1–5]. ASR generates a gel that swells in the presence of water, causing volumetric expansion and distress in the affected material. Moreover, the *microscopic/macroscopic* distress degree and features of the ASR depend upon the type (i.e. fine and coarse aggregate) and reactivity of the aggregates used, the amount of alkalis of the concrete, the temperature and relative humidity of the environment along with the exposure and confinement (i.e. reinforcement ratio, etc.) conditions of a given structure/structural member [4,6–11]. Over the years, authors [12–19] have studied the mechanisms that may trigger ASR-induced expansion and damage. Overall, ASR development may be summarized in three steps: (1) interaction of the alkaline environment and dissolution of the metastable siliceous phases from the aggregates; (2) the production of ASR-gel with the increase of alkali concentration within the aggregate particles and; (3) osmotic moisture absorption and gel expansion.

During ASR, an electrical double layer of cations (sodium, potassium and/or calcium) develops at the silica surface to offset its negative charge. Later on, the interaction between both phases (amorphous silica and alkali layers) will initially form a colloidal suspension and then, the reactive phases of the aggregates will start dissolving and precipitating ASR-gel, depending on the availability of the solvent, pore solution features, concentration, and structure, and the conditions to which it is exposed [20]. It has been found that the formation of the outer layer of cations starts hindering the silica uptake over time. However, the diffusion of alkaline ions is barely affected, and thus the chemical reaction continues, especially within the aggregate particles [12–19]. Once the increase of ASR-gel volume is constrained, the internal pressure increases up to the point where cracks take place within the aggregates [7]. The cracks develop in the reactive aggregate particles first at lower expansion levels (i.e.: < 0.05%) and then extend into the cement paste as ASR reaction/expansion progresses [3,7,9]. The developed internal pressure can be released due to the viscous behaviour of ASR-gel, which may permeate the

surrounding porous locations (e.g interfacial transition zone – ITZ) and cement paste. Moreover, different features (viscosity and chemistry) of the reaction products are found at different locations; i.e. alkali-silica gel (normally crystalline) within the aggregates and calcium-alkali-silica gel (normally amorphous) in the surrounding cement paste [15,21–24].

As the reaction progresses, calcium ions also diffuse into the silica particle, releasing Na^+ and K^+ to continue reacting with further siliceous phases. ASR-gel composition is significantly bulkier than the lime-alkali-silica composition; therefore, ASR-induced cracking initiates within the aggregates [15,21–24]. However, the chemical composition and structure of ASR-gel vary according to the alkalis involved in the reaction and depend on whether the gel has formed close to the surface or within the aggregate, which also changes its mechanical properties [1,25–29]. It has been argued that the presence of portlandite (or other soluble sources of calcium) is essential to form ASR-gel [13,15,30–32]; otherwise, siliceous phases remain in the solution. Moreover, the composition of ASR-gel is known to change with time; increasing in Ca/Si and decreasing in Na/Si.

An understanding of the elastic properties of ASR-gel is important to predict and prevent damage in concrete structures and structural components; especially because real structures display distinct exposure conditions and confinement effects from laboratory environments, which are known to play an important role in ASR-gel formation and features such as mechanical properties. However, measuring the mechanical properties of ASR-gel is quite difficult due to its amorphous nature [32]. As stated by Murtagh et al. [33], E-modulus of synthesized silica gels may reach values between 6.6 and 10.0 GPa and the bulk modulus of synthesized alkali–calcium–silica gels can range from 4 to 8 GPa at low $Ca(OH)_2$ content (0.08 M, average E-modulus ≈ 11.5 GPa) to 13–23 GPa at a high $Ca(OH)_2$ content (0.8 M, average E-modulus ≈ 34.5 GPa) [34,35].

1.1 Techniques for assessing AAR damage in concrete

1.1.1 Stiffness Damage Test (SDT)

The Stiffness Damage Test (SDT) was first developed by Walsh (1965) for evaluating the quality of rocks specimens [36], being afterwards adapted for assessing concrete by Crouch [37]. The test procedure is based on a cyclic loading (in compression) of concrete specimens and is able to quantify the degree of damage or physical integrity of distressed concrete. Both researchers selected the use of fixed loads of either 5.5 or 10 MPa, respectively, at a loading rate of 0.10 MPa. The outcomes of the SDT are the modulus of elasticity, the hysteresis area or the dissipated energy (hysteresis area), the plastic deformation and the non-linearity index (NLI) [3,8].

Details on the test procedure and specific considerations on its application as a diagnostic tool for assessing ASR-affected concrete can be found in Sanchez et al. [3,38]. The method was found very promising for assessing AAR damage and progress in concrete and the authors indicated that 40% of the concrete design strength provided the best correlation between SDT output parameters (Stiffness Damage Index – SDI, Plastic Deformation Index - PDI and also Non-Linearity Index - NLI) and the expansion of the ASR-affected concrete. However, since in most practical cases the 28-day strength of ageing concrete structures is unknown, Sanchez [3] suggested that the most suitable approach would be to first determine the compressive strength on cores extracted from locations that are not/less damaged in the structural member under investigation and then use 40% of this value for stiffness damage testing.

1.1.2 Damage Rating Index (DRI)

The Damage Rating Index (DRI) is a semi-quantitative microscopic analysis performed using a stereomicroscope (about 15-16 x magnification) where the petrographic damage features associated with AAR are counted through a grid of 1 cm² (i.e., 10 × 10 mm units) drawn on the surface of a polished concrete section [9,39]. The number of counts corresponding to each type of petrographic characteristics is then multiplied by a set of weighting factors, whose purpose is to balance their relative importance towards the distress mechanism. The final DRI value is normalized to an area of 100 cm²; overall the higher the DRI number, the greater the deterioration of affected concrete [3,7,9]. The DRI is rather a complementary petrographic tool aiming at quantifying the "damage degree" between different members from an affected structure or as a function of time within a specific concrete member.

A complete review of the DRI development and specific considerations on its application are given in Sanchez et al. [3,7,9]. The authors used the DRI to evaluate AAR distress with a wide range of reactive aggregates, different concrete strengths (25-45 MPa) and expansion levels (0.05% to 0.30%). It was

found that the DRI is a powerful tool to detect AAR damage/progress in concrete whatever the aggregate type and concrete strength used, mainly when the aggregate particles are analyzed down to 1 mm.

1.1.3 Compressive strength technique (CS)

Compressive strength is commonly used for structural concrete design. Yet, several past studies also aimed to use it to quantify AAR damage and development with more or less success. In AAR affected concrete, the compressive strength is a mechanical property that is the least affected by the chemical reaction due to AAR microscopic features (i.e. mainly cracks within the aggregate particles). Significant reductions in compressive strength are only observed for high and very high expansion levels (i.e. >0.20%) as by [4,40] which disables its use for diagnostic purposes.

1.1.4 Direct Shear Strength technique (DSS)

Shear strength in concrete is a property governed by tension and compression forces. Once cracked (and concrete will always present a certain amount of inner cracks, flaws, etc.), concrete may transfer shear forces across the cracks through two distinct mechanisms: a) dowel effect and; b) shear friction [41]. A number of test methods have been developed over the years to evaluate the direct shear capacity and shear friction of reinforced and unreinforced concrete [42–44].

De Souza et al. [45] evaluated AAR-induced expansion and damage on the direct shear strength of affected concrete and developed a simple, yet reliable setup to assess AAR progress in the laboratory. The authors found that the AAR significantly influences the direct shear strength of affected concrete as a function of its development. Moreover, the impact of the AAR on the shear strength was more significant for low (0.05%) and moderate (0.12%) expansions. The proposed shear setup showed to be a fast and promising tool for detecting AAR-induced expansion and damage in the laboratory. Yet, only AAR-affected laboratory samples fabricated and monitored under accelerated and free expansion conditions were tested in this program [45].

1.2 Micro-Indentation

Indentation hardness testing has been used to evaluate the mechanical properties of materials [35,46–49]. More recently, the advent of nano- and micro-scale science, engineering and technology, coupled with substantial progress in instrumentation, has resulted in depth-sensing indentation [50]. A typical measurement via an indenter can record load and displacements from the surface of a material. Amongst these properties, the elastic modulus, E, and hardness, H, are timely obtainable without complicated testing apparatus [50]. The micro-hardness is an important index reflecting the mechanical properties of the material. The principle of the indentation, or Vickers hardness tester, is pressing the diamond corner-cone indenter with a certain shape into the surface of the tested piece under a certain test force [46,47,49]. The test force is maintained for a preset time and then, removed. The two diagonal lengths of the indentation are measured, and the hardness can be obtained from these lengths.

Indentation has been used in concrete samples in recent years; in general, to assess the mechanical properties of the ITZ and distinct phases of the samples, such as in recycled concrete, different properties of ITZs and mortars [46,47,49]. The E-modulus of various hydrated phases has been determined using different indentation techniques [35]. The microhardness tests were used to study the bulk properties of cement paste with a maximum penetration depth at the level of 10^{-5} m [51]. As the area of the indenter is larger than the size of homogenous regions of single hydrates [52–54], micro-indentation is only able to deliver data on hydrate assemblages in cement paste, for which an E-modulus in the range of 10–30 GPa were found [52–54]. With the significant advances in the conventional Vickers microhardness technique, a novel micro indentation method was developed to investigate the elastic modulus and the micro-strength of ITZ in reinforced concrete [51–53].

2. SCOPE OF THE WORK

As stated above, a number of techniques have been developed in the past aiming to assess ASR-induced damage development in concrete. Furthermore, it is anticipated that ASR-gel features such as mechanical properties may influence the damage generation and propagation in concrete, especially in field structures/structural components presenting a wide range of exposure conditions and confinement effects. However, there is currently very limited information in the literature in this regard. This research project presents the results of a multi-level assessment of ASR-induced damage development and focuses on the distress generated at distinct locations of affected concrete: aggregate particles, ITZ and

cement paste. The latter is expected to aid in the understanding of the material's deterioration as a function of ASR development.

3. MATERIALS AND METHODS

3.1 Materials and mixture proportions

Concrete specimens presenting a highly reactive coarse aggregate (Springhill greywacke) were fabricated in the laboratory. The coarse aggregate ranged from 5 to 20 mm in size. Non-reactive fine aggregate (NF) were also used in combination with the reactive coarse for concrete manufacturing. Table 3.1 provides information on the different aggregates used in this study.

Table 3.1: Reactive (R) and non-reactive (NR) aggregates used in the research.

Aggregate		Reactivity	Rock Type	Specific gravity	Absorption (%)	AMBT[a] (%)
Coarse	SPH	R	Crushed Greywacke	2.73	0.71	0.33
Fine	NF	NR	Natural derived from granite	2.67	0.82	0.08
Results at 14 days of curing of the AMBT (ASTM C 1260) carried out on the aggregates selected.						

A conventional Portland cement (CSA Type GU, ASTM type 1) containing high alkali content (0.88% Na2Oe) was used in the mixture. Reagent grade NaOH was used to raise the total alkali content of the mixtures to 1.25% Na_2O_{eq} by cement mass, for accelerating the AAR expansion process. Table 3.2 provides information on the chemical composition of the general use of Cement used in this study. The concrete mixture (Table 3.3) was mix-proportioned as per ASTM C1293.

Table 3.2: Chemical composition of the Portland cement.

Material	CaO	SiO_2	Al_2O_3	Fe_2O_3	SO_3	MgO	$Na_2O_{eq.}$	LOI
GU Cement	61.93	20.1	5.03	3.80	4.38	2.42	0.91	2.91

Table 3.3: Concrete mix-design as per ASTM C1293.

Mixture	w/cm = 0.45		Aggregates (kg/m^3)	
	Water (kg/m^3)	Cement (kg/m^3)	NR Fine	SPH
SPH Control	189	420	836	938

3.2 Manufacture of the concrete specimens

Thirty-six cylinders, 100 × 200 mm in size, were fabricated in the laboratory. After 24 h, the samples were demoulded and stored in a moist curing room for another 24 h. Then, small holes (5 mm in diameter by 15 mm deep) were drilled at the two flat ends of the samples, in which steel gauge studs were glued in place with a fast-setting cement slurry, for longitudinal expansion measurements. Next, the samples were left to harden over 5 days before the "0" reading was taken; all samples were finally placed in sealed plastic buckets lined with a damp cloth and stored at 38 °C and 100% R.H.

The ASR-affected cylinders were monitored for length variations until they reach different expansion levels (i.e. 0.00%, 0.05%, 0.13% and 0.22%). As per ASTM C 1293, the buckets were cooled down to 23 °C for 16 ± 4 h prior to the periodic measurements. Then, when the cylinders reach the specified expansion levels, they were wrapped in plastic film and kept under 12 °C to inhibit further AAR deterioration until all tests are conducted (due to testing capacity issues). Companion and "sound" concrete specimens, incorporating lithium nitrate (i.e. 0.74 Li/[Na+K] ratio) to avoid further ASR-induced development, were also manufactured at the same time and stored in the moist curing chamber for over 28 days, prior being mechanically tested (i.e. compressive and shear strength along with modulus of elasticity).

3.3 Assessment of the ASR development in the concrete

3.3.1 Stiffness Damage Test (SDT)

Three cylinders of each concrete mixture at 90 days of exposure were subjected to five cycles of loading/unloading at a controlled loading rate of 0.10 MPa/s. The SDT procedure was performed following Sanchez et al. publications [3,38,40], i.e. using a loading level corresponding to 40% of the 28-day concrete strength. To characterize all mixtures at 28 days compressive strength, samples were wrapped and placed at 12 °C, since some of the specimens contained highly reactive aggregates and ASTM C 39 method could not be followed as they could develop some ASR. The cylinders were maintained at 12 °C for a 47-day period, according to the maturity concept as by ASTM C 1074.

3.3.2 Damage Rating Index (DRI)

A semi-quantitative petrographic analysis, using the DRI, was performed on one specimen from each concrete mixture at the specific expansion levels, according to the method described by Sanchez [3,9]. The DRI final number presented hereafter is the normalized 100 cm² value obtained over polished concrete specimens.

3.3.3 Compressive Strength Test

Compressive strength was measured through two different approaches with different and specific goals. First, as previously mentioned, the 28 days compressive strength of each mixture was obtained considering the maturity concept as by ASTM C 107 to gather the 28-day ultimate capacity of the mix. The second compressive strength measurements were carried out on three cylinders used for stiffness damage testing, to verify the compressive strength loss of the material as ASR develops. This procedure was adopted and considered valid after Sanchez et al. [3,9] confirmed the largely non-destructive character of the SDT.

3.3.4 Direct Shear Test

The direct shear test was performed according to the method and setup proposed by Barr and Hasso [55] and adapted for damaged concrete as per De Souza et al. [11]. The same approach considering the maturity concept was used to characterize the "zero" reading for all concrete mixtures at equivalent 28 days. At 90 days of exposure, three samples of each concrete mixture were selected, however, differently from CS, stiffness damage test was not performed on the samples previous the direct shear test. Before testing, all samples were carefully ground so that a circumferential notch was created [11,55]. The notch depth was adopted as about 20 mm ± 3 mm to ensure a shear-type failure without leaving a too-small area of the sample to be tested.

3.3.5 Micro-Indentation

Standard Vickers hardness tests were conducted on samples carefully polished (two samples of 2x2 cm in size per expansion level) using oil containing diamond powders, without previous drying or any type of impregnation. The remaining half of the samples from DRI tests were carefully inspected through the stereomicroscope to localize the most damaged locations with the presence of gel. The indentation was conducted at a maximum of 48 h after polishing using a diamond indenter and 0.09807 N (100 mN) load for Vickers indentations (Struers Duramin Machine) at all expansion levels. A dwell time of 10 s and a total of 4 points were measured to obtain the Vickers micro-hardness average values to cover statistics. The test scheme for the VH test is shown in Figure 3.1.
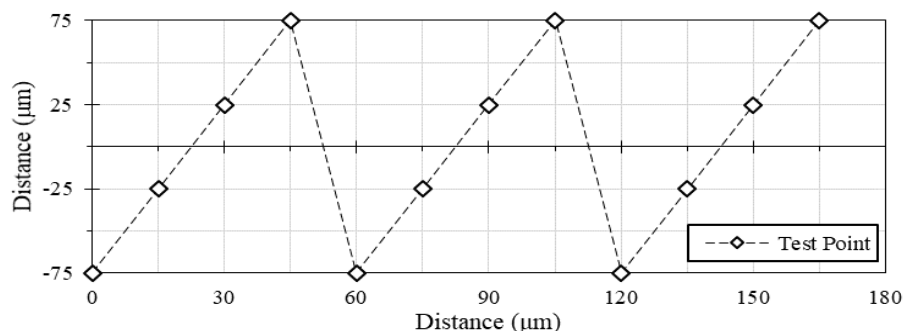

Figure 3.1: Schematic diagram of the distribution of test points in the Vickers hardness test.

4. RESULTS AND DISCUSSIONS

4.1 ASR Kinetics

In this section, ASR expansion kinetics and amplitude results are presented. Figure 4.1 shows the average expansion and mass variation values obtained. The mixtures containing the Springhill coarse aggregate (SPH) displayed a very high reactivity, reaching 0.22% in 90 days; lower expansion levels of 0.05% and 0.13% were obtained after 25 and 45 days, respectively. The mass gain ranged from 0.31% for 0.05% of expansion to 0.66% at the maximum expansion level.
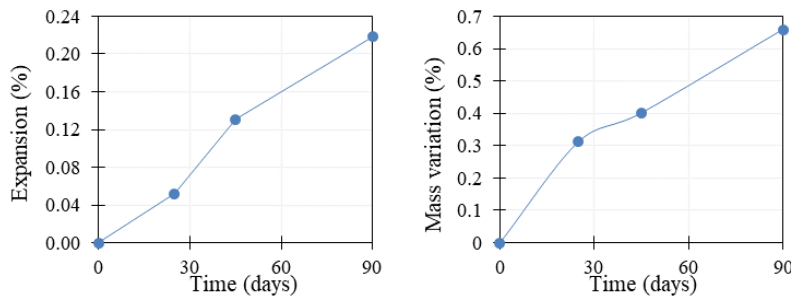

Figure 4.1: Expansion and mass variation of ASR-affected concrete specimens.

4.2 Mechanical Properties Assessment

Figure 4.2 shows the reductions in modulus of elasticity, shear strength and compressive strength of the SPH concrete investigated in this work (their respective average data are dosplayed in Table 4.1). The data presented here are the variation ratio of values obtained at each selected "free" expansion level against the values obtained on companion sound concrete specimens tested at 28 days. The direct shear test results according to the last findings by De Souza et al. [11] were assessed and the modulus of elasticity was obtained through the SDT method as per Sanchez et al. [3,38,40]. In the plots, values of 0.0 mean 0% loss whereas values of 1.00 mean 100% reduction.
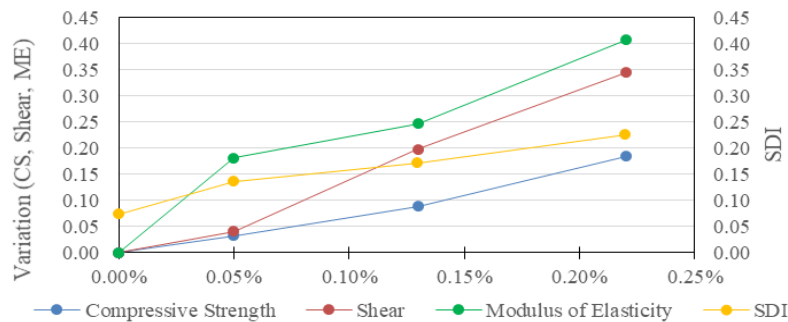

Figure 4.2: Variation ratio among the mechanical properties (Compressive, Shear Strength and Modulus of Elasticity) and Stiffness Damage Index (SDI) of ASR-affected concrete specimens.

Table 4.1: Obtained values for the mechanical properties tests (Compressive, Shear Strength and Modulus of Elasticity) and Stiffness Damage Index (SDI) of sound and ASR-affected concrete specimens.

Samples	Fc (MPa)	Shear (MPa)	E (GPa)	SDI
Sound Concrete at 28* days	38.5	9.8	28.8	0.08
0.05% of expansion	37.8	9.4	23.6	0.14
0.13% of expansion	34.3	5.7	18.2	0.17
0.22% of expansion	30.7	5.4	15.8	0.23

* maintained at 12 °C for a 47-day period, according to the maturity concept as by ASTM C 1074.

In general, compressive strength (CS) was found to decrease in a somewhat modest way in comparison with the other mechanical properties tested. For samples with low expansion levels, the compressive strength losses ranged from 3% to 18%, for 0.05% and 0.22% of expansion. In the direct shear strength (DSS) results of the affected samples, it is seen that all mixtures present a shear strength decrease as a function of ASR-induced expansion; the losses ranged from 4%, 20% and 35% for the expansion levels of 0.05%, 0.13% and 0.22%, respectively. Direct shear reductions seem to be more important when the matrix starts to have a higher amount of cracks as a result of the higher expansion levels, facilitating the propagation of cracks during the performance of the test.

The most affected mechanical property was the modulus of elasticity. The loss plot ranges from 18% (0.05% of expansion) to 45% (0.22% of expansion). As well known in the literature [8,56–60] for conventional concrete, the modulus of elasticity is largely governed by the mechanical properties of the aggregates, especially the coarse aggregate. Therefore, this phenomenon is likely responsible for the significant decrease in ME of the ASR-affected mixtures. Moreover, SDI results were obtained in this work through the *stiffness damage test* (SDT) method, per Sanchez et al. [3,38,40]. SDI values were found to range from about 0.08 at 0.00% of expansion to 0.23 at 0.23%. The development of cracks within the aggregate particles and the propagation through the cement paste leads to an extension of inner damage of the affected concrete. Therefore, the affected material releases a significant amount of energy while he cracks closure over the compressive SDT cycles, which results in the important raise of SDI values.

4.3 Microscopy Assessment

Figure 4.3 presents the microscopic damage features and DRI numbers obtained from the ASR-affected concrete specimens. Globally, it is possible to see that all DRI numbers increase as a function of the specimens' expansions. The latter happens due to the generation of the cracks within the aggregate particles (i.e. low and moderate levels) and the cement paste (high and very high levels) throughout the physicochemical process. Greater DRI numbers are found at 0.22% of expansion (723), followed by 0.13% (399), 0.05% (214) and for sound concrete 0.00% of expansion (132), which is in agreement with the Shear Strength, Modulus of Elasticity and SDI results.

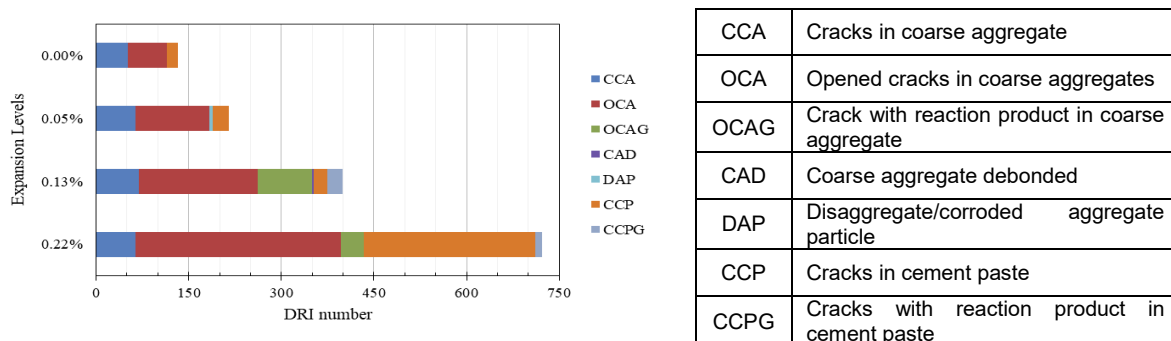|	
CCA	Cracks in coarse aggregate
OCA	Opened cracks in coarse aggregates
OCAG	Crack with reaction product in coarse aggregate
CAD	Coarse aggregate debonded
DAP	Disaggregate/corroded aggregate particle
CCP	Cracks in cement paste
CCPG	Cracks with reaction product in cement paste

Figure 4.3: Damage Rating Index for the ASR-affected concrete specimens.

As discussed in the literature [4,6,7,40], in samples with lower expansion levels (i.e. 0.00% and 0.05%) due to ASR, cracks can be found inside the aggregate particles and it is unlikely to find cracks in the cement paste extending from aggregates. However, at 0.13% of expansion, the cracks propagate and reach the cement paste; besides, a significant amount of ASR-gel was found in the sample. At 0.22% of expansion, the cracks formed within the aggregate propagate through the cement paste and connect to each other, indicating an extension of the cracking network within the concrete matrix.

4.4 Micro-indentation

The Vickers hardness average values at the four different expansion levels are shown in Figure 4.4, where a) were taken within the aggregate particle and passing through prior selected cracks. Otherwise, b) were taken starting in the aggregate, passing through the ITZ and finishing at the cement paste; however, avoiding visually damaged coarse aggregate particles. It is important to be mentioned that for a), the selected cracks for 0.00% and 0.05% of expansion were closed cracks without the presence of ASR-gel, while for 0.13% and 0.22% of expansion, the selected cracks were opened (i.e. crack width average of 140 μm) and filled with ASR-gel.
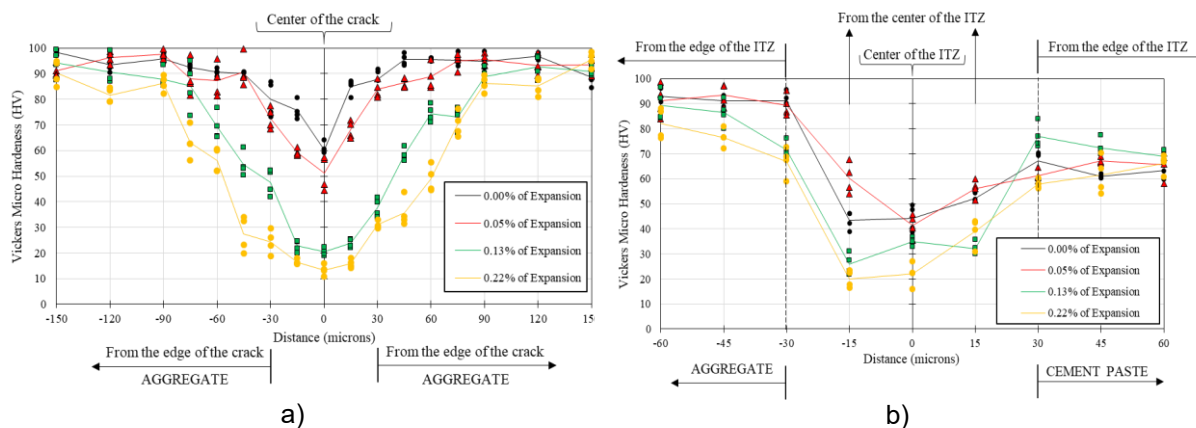
Figure 4.4: Vickers micro-hardness profile: a) within the aggregate and passing through selected cracks; b) starting in the aggregate, passing through the ITZ and finishing at cement paste.

The above results showed in a) indicate that the higher the expansion levels, the lower the values of Vickers' Micro Hardness at the centre of the crack (i.e. 60.1, 51.3, 20.5 and 13.4 for 0.00%, 0.05%, 0.13% and 0.22% of expansion, respectively). Moreover, the farther the indentation from the edge of the cracks, the higher the values gathered. The reaction between alkalis and the metastable silica to form ASR-gel seems to increase the porosity of the particles, especially at locations close to the crack edges. In other words, ASR development decreases the surface hardness of the material, also changing its local modulus of elasticity. Likewise, as seen in Figure 4.4.b), the closer to the aggregates boarders, the lower the HV values, indicating an increase in damage to the region. Moreover, the higher the expansion level, the lower the HV values. Yet, at the ITZ, the HV values also seem to be influenced accordingly with the expansion level. But the same is not seen at the cement paste, at least on the evaluated points. Furthermore, within the ITZ, the HV values are slightly lower in points closer to aggregates, which may indicate that the ASR development is changing the ITZ microstructure.

The mechanical properties of the ASR-gel measured through the micro indentation on the polished and undried samples are presented in Figure 4.5. The test was only conducted on samples presenting 0.13% and 0.22% expansion since it was necessary to have a significant amount of gel in the samples. The Vickers' hardness values were, on average, 23.8 and 17.4 within the aggregate particle for 0.13% and 0.22% of expansion, respectively. On the edge of the aggregate/ITZ, the highest values were obtained in samples with 0.22% expansion (i.e. 101.5); in the cement paste, the HV values for 0.22% kept higher than 0.13%, on average 67.5 for 0.22% and 55.7 for 0.13% expansion.
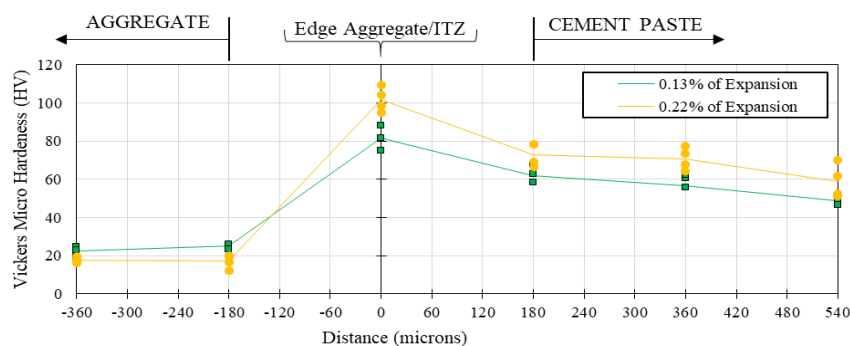

Figure 4.5: Vickers micro-hardness profile on ASR-gel through aggregate/ITZ/cement paste

Through the aggregate towards the edge and close to the cement paste, it seems that the structure of the ASR-gel changes significantly its properties, which can be caused by an increase in calcium content in the gel composition [35]. In all aggregates, there is a trend to considerably increase HV values close to the edge of the aggregates. The maximum values measured are 109.2 and 103.9 HV. However, the farther from the ITZ in the cement paste, the lower the HV values.

5. CONCLUSIONS

The primary objective of this research program was to present the results of a multi-level analysis on ASR affected concrete presenting distinct expansion levels and damage degrees. Moreover, the important emphasis was given to the understanding of the induced damage at distinct locations of the affected concrete, including the analysis of ASR-gel features. From the results obtained in this study, the following conclusions may be drawn:

- The development of ASR significantly influences the mechanical properties (i.e. compressive strength-CS, shear strength-SS, modulus of elasticity-ME and stiffness damage index-SDI) of the affected concrete as a function of its development, as expected. Reduction values ranging between 3% to 18% for CS and from 18% to 41% for ME from lower o higher expansion levels;

- Microscopic investigations showed that the development of ASR distress results in the formation of cracks within the reactive aggregate particles and propagate through the cement paste at advanced levels of expansion.

- Micro-indentation results showed that the development of ASR reduces significantly the mechanical properties of affected aggregates. Within the same aggregate, Vickers' hardness (HV) values change significantly as a function of the distance of the crack and expansion level, indicating inner damage in the aggregate structure. Moreover, the same behaviour was found in the regions close to the edge aggregate/ITZ, as the higher were the expansion level, the lower the HV values.

- The evaluation of ASR-gel through micro-indentation indicates that whenever within the aggregates, ASR-gel presents lower HV values, lower than the values found when the gel is in contact with the cement paste. However, at the interface aggregate/ITZ, the highest HV values were found. This highlights the importance of a better understanding of ASR-gel features for assessing damage and developing models to predict ASR-induced distress development.

6. ACKNOWLEDGEMENTS

7. REFERENCES

[1] J. Lindgård, Ö. Andiç-Çakir, I. Fernandes, T.F. Rønning, M.D.A. Thomas, Alkali-silica reactions (ASR): Literature review on parameters influencing laboratory performance testing, Cem. Concr. Res. 42 (2012) 223–243. doi:10.1016/j.cemconres.2011.10.004.

[2] M. Rashidi, M.C.L. Knapp, A. Hashemi, J.Y. Kim, K.M. Donnell, R. Zoughi, L.J. Jacobs, K.E. Kurtis, Detecting alkali-silica reaction: A multi-physics approach, Cem. Concr. Compos. 73 (2016) 123–135. doi:10.1016/j.cemconcomp.2016.07.001.

[3] L.F.M. Sanchez, Contribution to the assessment of damage in aging concrete infrastructures affected by alkali-aggregate reaction, (2014) 341.

[4] L.F.M. Sanchez, B. Fournier, M. Jolin, D. Mitchell, J. Bastien, Overall assessment of Alkali-Aggregate Reaction (AAR) in concretes presenting different strengths and incorporating a wide range of reactive aggregate types and natures, Cem. Concr. Res. 93 (2017) 17–31. doi:10.1016/j.cemconres.2016.12.001.

[5] B. Fournier, M.-A. Bérubé, Alkali-aggregate reaction in concrete: a review of basic concepts and engineering implications, Can. J. Civ. Eng. 27 (2000) 167–191. doi:10.1139/cjce-27-2-167.

[6] L. Sanchez, Contribution to the assessment of damage in aging concrete infrastructures affected by alkali-aggregate reaction, UNIVERSITE LAVAL, 2014.

[7] L.F.M. Sanchez, B. Fournier, M. Jolin, J. Duchesne, Reliable quantification of AAR damage through assessment of the Damage Rating Index (DRI), Cem. Concr. Res. 67 (2015) 74–92. doi:10.1016/j.cemconres.2014.08.002.

[8]   L.F.M. Sanchez, B. Fournier, M. Jolin, J. Bastien, Evaluation of the stiffness damage test (SDT) as a tool for assessing damage in concrete due to ASR: Test loading and output responses for concretes incorporating fine or coarse reactive aggregates, Cem. Concr. Res. 56 (2014) 213–229. doi:10.1016/j.cemconres.2013.11.003.

[9]   L.F.M. Sanchez, B. Fournier, M. Jolin, M.A.B. Bedoya, J. Bastien, J. Duchesne, Use of Damage Rating Index to quantify alkali-silica reaction damage in concrete: Fine versus coarse aggregate, ACI Mater. J. 113 (2016) 395–407. doi:10.14359/51688983.

[10]   L.F.M. Sanchez, B. Fournier, M. Jolin, J. Bastien, D. Mitchell, Practical use of the Stiffness Damage Test (SDT) for assessing damage in concrete infrastructure affected by alkali-silica reaction, Constr. Build. Mater. 125 (2016) 1178–1188. doi:10.1016/j.conbuildmat.2016.08.101.

[11]   D.J. De Souza, L.F.M. Sanchez, M.T. De Grazia, Evaluation of a direct shear test setup to quantify AAR-induced expansion and damage in concrete, Constr. Build. Mater. 229 (2019). doi:10.1016/j.conbuildmat.2019.116806.

[12]   M. Cyr, R. Pouhet, Resistance to alkali-aggregate reaction (AAR) of alkali-activated cement-based binders, Woodhead Publishing Limited, 2015. doi:10.1533/9781782422884.3.397.

[13]   F. Rajabipour, E. Giannini, C. Dunant, J.H. Ideker, M.D.A. Thomas, Alkali-silica reaction: Current understanding of the reaction mechanisms and the knowledge gaps, Cem. Concr. Res. 76 (2015) 130–146. doi:10.1016/j.cemconres.2015.05.024.

[14]   E.R. Latifee, State-of-the-Art Report on Alkali Silica Reactivity Mitigation Effectiveness Using Different Types of Fly Ashes, J. Mater. 2016 (2016) 1–7. doi:10.1155/2016/7871206.

[15]   A. Gholizadeh-Vayghan, F. Rajabipour, The influence of alkali–silica reaction (ASR) gel composition on its hydrophilic properties and free swelling in contact with water vapor, Cem. Concr. Res. 94 (2017) 49–58. doi:10.1016/j.cemconres.2017.01.006.

[16]   S. Diamond, Alkali silica reactions - Some paradoxes, Cem. Concr. Compos. 19 (1997) 391–401. doi:10.1016/s0958-9465(97)00004-8.

[17]   S. Diamond, A review of alkali-silica reaction and expansion mechanisms 1. Alkalies in cements and in concrete pore solutions, Cem. Concr. Res. 5 (1975) 329–345. doi:10.1016/0008-8846(75)90089-7.

[18]   D.W. Hobbs, W.H. Gutteridge, A. Samarin, Particle size of aggregate and its influence upon the expansion caused by the alkali-silica reaction, Mag. Concr. Res. 32 (1980) 251–252. doi:10.1680/macr.1980.32.113.251.

[19]   H. Wang, J.E. Gillott, Mechanism of alkali-silica reaction and the significance of calcium hydroxide, Cem. Concr. Res. 21 (1991) 647–654. doi:10.1016/0008-8846(91)90115-X.

[20]   M. Prezzi, P.J.M. Monteiro, G. Sposito, The alkali-silica reaction, part I: Use of the double-layer theory to explain the behavior of reaction-product gels, ACI Mater. J. 94 (1997) 10–17. doi:10.14359/280.

[21]   S. Chatterji, N. Thaulow, A.D. Jensen, Studies of alkali-silica reaction. part 5. Verification of a newly proposed reaction mechanism, Cem. Concr. Res. 19 (1989) 177–183. doi:10.1016/0008-8846(89)90081-1.

[22]   Y. Kawabata, K. Yamada, The mechanism of limited inhibition by fly ash on expansion due to alkali–silica reaction at the pessimum proportion, Cem. Concr. Res. 92 (2017) 1–15. doi:10.1016/j.cemconres.2016.11.002.

[23]   C. Balachandran, J.F. Muñoz, T. Arnold, Characterization of alkali silica reaction gels using Raman spectroscopy, Cem. Concr. Res. 92 (2017) 66–74. doi:10.1016/j.cemconres.2016.11.018.

[24]   S. Abbas, S.M.S. Kazmi, M.J. Munir, Potential of rice husk ash for mitigating the alkali-silica reaction in mortar bars incorporating reactive aggregates, Constr. Build. Mater. 132 (2017) 61–70. doi:10.1016/j.conbuildmat.2016.11.126.

[25]   X. Hou, L.J. Struble, R.J. Kirkpatrick, Formation of ASR gel and the roles of C-S-H and portlandite, Cem. Concr. Res. 34 (2004) 1683–1696. doi:10.1016/j.cemconres.2004.03.026.

[26] M. Kawamura, H. Fuwa, Effects of lithium salts on ASR gel composition and expansion of mortars, Cem. Concr. Res. 33 (2003) 913–919. doi:10.1016/S0008-8846(02)01092-X.

[27] M. Beyene, A. Snyder, R.J. Lee, M. Blaszkiewicz, Alkali Silica Reaction (ASR) as a root cause of distress in a concrete made from Alkali Carbonate Reaction (ACR) potentially susceptible aggregates, Cem. Concr. Res. 51 (2013) 85–95. doi:10.1016/j.cemconres.2013.04.014.

[28] A.K. Saha, M.N.N. Khan, P.K. Sarker, F.A. Shaikh, A. Pramanik, The ASR mechanism of reactive aggregates in concrete and its mitigation by fly ash: A critical review, Constr. Build. Mater. 171 (2018) 743–758. doi:10.1016/j.conbuildmat.2018.03.183.

[29] X. Feng, M.D.A. Thomas, T.W. Bremner, K.J. Folliard, B. Fournier, New observations on the mechanism of lithium nitrate against alkali silica reaction (ASR), Cem. Concr. Res. 40 (2010) 94–101. doi:10.1016/j.cemconres.2009.07.017.

[30] Š. Šachlová, A. Burdová, Z. Pertold, R. Přikryl, Macro- and micro-indicators of ASR in concrete pavement, Mag. Concr. Res. 63 (2011) 553–571. doi:10.1680/macr.2011.63.8.553.

[31] S. Chatterji, The role of Ca(OH)2 in the breakdown of Portland cement concrete due to alkali-silica reaction, Cem. Concr. Res. 9 (1979) 185–188. doi:10.1016/0008-8846(79)90024-3.

[32] J. Moon, S. Speziale, C. Meral, B. Kalkan, S.M. Clark, P.J.M. Monteiro, Determination of the elastic properties of amorphous materials: Case study of alkali-silica reaction gel, Cem. Concr. Res. 54 (2013) 55–60. doi:10.1016/j.cemconres.2013.08.012.

[33] M.J. MURTAGH, E.K. GRAHAM, C.G. PANTANO, Elastic Moduli of Silica Gels Prepared with Tetraethoxysilane, J. Am. Ceram. Soc. 69 (1986) 775–779. doi:10.1111/j.1151-2916.1986.tb07358.x.

[34] J.W. Phair, S.N. Tkachev, M.H. Manghnani, R.A. Livingston, Elastic and structural properties of alkaline-calcium silica hydrogels, J. Mater. Res. 20 (2005) 344–349. doi:10.1557/JMR.2005.0061.

[35] A. Leemann, P. Lura, E-modulus of the alkali-silica-reaction product determined by micro-indentation, Constr. Build. Mater. 44 (2013) 221–227. doi:10.1016/j.conbuildmat.2013.03.018.

[36] J.B. Walsh, The effect of cracks on the uniaxial elastic compression of rocks, J. Geophys. Res. 70 (1965) 399–411. doi:10.1029/JZ070i002p00399.

[37] R.S. Crouch, Specification for the determination of stiffness damage parameters from the low cyclic uniaxial compression of plain concrete cores, 1987.

[38] L.F.M. Sanchez, B. Fournier, M. Jolin, J. Bastien, Evaluation of the Stiffness Damage Test (SDT) as a tool for assessing damage in concrete due to alkali-silica reaction (ASR): Input parameters and variability of the test responses, Constr. Build. Mater. 77 (2015) 20–32. doi:10.1016/j.conbuildmat.2014.11.071.

[39] V. Villeneuve, B. Fournier, Determination of the damage in concrete affected by ASR–the damage rating index (DRI), in: 14th Int. Conf. Alkali-Aggregate React. Concr., Austin (Texas), 2012: p. electronic.

[40] L.F.M. Sanchez, T. Drimalas, B. Fournier, D. Mitchell, J. Bastien, Comprehensive damage assessment in concrete affected by different internal swelling reaction (ISR) mechanisms, Cem. Concr. Res. 107 (2018) 284–303. doi:10.1016/j.cemconres.2018.02.017.

[41] M. Haskett, D.J. Oehlers, M.S. Mohamed Ali, S.K. Sharma, Evaluating the shear-friction resistance across sliding planes in concrete, Eng. Struct. 33 (2011) 1357–1364. doi:10.1016/j.engstruct.2011.01.013.

[42] L. Banks-Sills, M. Arcan, An edge-cracked Mode II fracture specimen., Exp. Mech. 23 (1983) 257–261.

[43] D.F. Adams, D.E. Walrath, Current status of the Iosipescu shear test method., J. Compos. Mater. 21 (1987) 494–507.

[44] H.A. Richard, A new compact shear specimen, Int. J. Fract. 17 (1981) 5–7.

[45] D.J. De Souza, L.F.M. Sanchez, M.T. De Grazia, Evaluation of a direct shear test setup to quantify AAR-induced expansion and damage in concrete, Constr. Build. Mater. 229 (2019) 116806. doi:10.1016/j.conbuildmat.2019.116806.

[46] D.J. Shuman, A.L.M. Costa, M.S. Andrade, Calculating the elastic modulus from nanoindentation and microindentation reload curves, Mater. Charact. 58 (2007) 380–389. doi:10.1016/j.matchar.2006.06.005.

[47] B. Lu, C. Shi, Z. Cao, M. Guo, J. Zheng, Effect of carbonated coarse recycled concrete aggregate on the properties and microstructure of recycled concrete, J. Clean. Prod. 233 (2019) 421–428. doi:10.1016/j.jclepro.2019.05.350.

[48] W. Wu, R. Wang, C. Zhu, Q. Meng, The effect of fly ash and silica fume on mechanical properties and durability of coral aggregate concrete, Constr. Build. Mater. 185 (2018) 69–78. doi:10.1016/j.conbuildmat.2018.06.097.

[49] A. Nastic, A. Merati, M. Bielawski, M. Bolduc, O. Fakolujo, M. Nganbe, Instrumented and Vickers Indentation for the Characterization of Stiffness, Hardness and Toughness of Zirconia Toughened Al2O3 and SiC Armor, J. Mater. Sci. Technol. 31 (2015) 773–783. doi:10.1016/j.jmst.2015.06.005.

[50] J.H. Kim, T. Tabaru, H. Hirai, Evaluation technique of the hardness and elastic modulus of materials with fine microstructures, Mater. Trans. 44 (2003) 673–676. doi:10.2320/matertrans.44.673.

[51] H. Liu, X. Ren, J. Li, Indentation tests based multi-scale random media modeling of concrete, Constr. Build. Mater. 168 (2018) 209–220. doi:10.1016/j.conbuildmat.2018.02.050.

[52] P. Lura, P. Trtik, B. Münch, Validity of recent approaches for statistical nanoindentation of cement pastes, Cem. Concr. Compos. 33 (2011) 457–465. doi:10.1016/j.cemconcomp.2011.01.006.

[53] W. Zhu, P.J.M. Bartos, Application of depth-sensing microindentation testing to study of interfacial transition zone in reinforced concrete, Cem. Concr. Res. 30 (2000) 1299–1304. doi:10.1016/S0008-8846(00)00322-7.

[54] A. Leemann, L. Bernard, S. Alahrache, F. Winnefeld, ASR prevention - Effect of aluminum and lithium ions on the reaction products, Cem. Concr. Res. 76 (2015) 192–201. doi:10.1016/j.cemconres.2015.06.002.

[55] B. Barr, E.B.D. Hasso, Development of a compact cylindrical shear test specimen, J. Mater. Sci. Lett. 5 (1986) 1305–1308.

[56] R.S. Crouch, J.G.M. Wood, Damage evolution in AAR affected concretes, Eng. Fract. Mech. 35 (1990) 211–218. doi:10.1016/0013-7944(90)90199-Q.

[57] S. Dean, N. Smaoui, B. Bissonnette, M. Bérubé, B. Fournier, B. Durand, Mechanical Properties of ASR-Affected Concrete Containing Fine or Coarse Reactive Aggregates, J. ASTM Int. 3 (2006) 12010. doi:10.1520/JAI12010.

[58] N. Smaoui, B. Bissonnette, M. Bérubé, B. Fournier, B. Durand, Mechanical Properties of ASR-Affected Concrete Containing Fine or Coarse Reactive Aggregates, J. ASTM Int. 3 (2006) 12010. doi:10.1520/JAI12010.

[59] D.J. De Souza, L. Sanchez, F. Ahimoghadam, G. Fathifazl, Comparison Among Different Mix-Design Procedures for RCA Concrete, ACI Spec. Publ. SP-334 (2019) 99–121. https://www.concrete.org/publications/internationalconcreteabstractsportal.aspx?m=details&ID=51720255.

[60] D.J. Souza, L.Y. Yamashita, F. Dranka, M.H.F. Medeiros, R.A. Medeiros-Junior, Repair Mortars Incorporating Multiwalled Carbon Nanotubes: Shrinkage and Sodium Sulfate Attack, J. Mater. Civ. Eng. 29 (2017) 1–12. doi:10.1061/(ASCE)MT.1943-5533.0002105.